Transactions of the Materials Research Society of Japan 32[1] 287-292 (2007)

Functional Properties of Glycosphingolipid Aggregates and Mixtures with Cholesterol and Phospholipid

Mitsuhiro Hirai* and Teruaki Onai
Department of Physics, Gunma University, Maebashi 371-8510, Japan.
Fax: 81-272-220-7551, e-mail: mhirai@fs.aramaki.gunma-u.ac.jp

The structure and function of lipid microdomains in mammalian plasma membrane, so-called rafts are among the hot topics in cell biology, since these domains are assumed to be involved in important membrane-associated events, such as signal transduction, which were reported in physiological and immunological studies. Major components of rafts are glycosphingolipids (GSLs). Gangliosides are main species of GSLs and around 80 species are known. In spite of accumulation of amounts of evidence on the physiological functions of GSLs and rafts, the physicochemical properties of the structure and dynamics of membranes occluding GSLs have been less abundant and confuse. In these ten years we have been studying and clarified unique functional structural features by using synchrotron X-ray scattering and neutron elastic and quasi-elastic scattering techniques complementary. This report is focused on how to clarify and characterize lipid membrane interfaces by using solution X-ray and neutron scattering methods with referring our major findings on the structure and dynamics of GSLs and lipid mixtures containing GSLs as a model of rafts.
Key words: glycosphingolipid, raft, small-angle scattering, contrast variation

1. INTRODUCTION

Recently the presence and formation of lipid microdomains, so-called rafts [1], in mammalian plasma membrane have been attracting huge interests since these microdomains are assumed to play as a platform of important biological functions such as signal transduction, cell adhesion and lipid/protein sorting [2-6]. A common feature of plasma membrane microdomains is their peculiar lipid composition, being rich in glycosphingolipids (GSLs), sphingomyelin and cholesterol. Gangliosides, major components of GSLs, are acidic lipids composed of a ceramide linked to an oligosaccharide chain containing one or more sialic acid residues. Gangliosides are localized on the plasma membrane surface and to be rich in central nervous system. Functions of rafts are assumed to relate to the peculiar features of GSL molecules both in ceramide and oligosaccharide portions. The structures of some different types of representative gangliosides molecules are shown in Figure 1. The sugar head portion of ganglioside has an ability of formation of complex hydrogen bond network. In addition, as a common feature of sphingolipids, the tail portion of gangliosides acts as hydrogen bond acceptor as well as hydrogen bond donor, whereas that of glycerolipid acts only as hydrogen bond acceptor [7]. Due to this feature and an enrichment of oligosaccharides in hydrophilic moiety, GSLs are assumed to form complex networks of hydrogen bonding between those lipids and water molecules [8]. Thus the physiological functions of GSL microdomains are assumed to deeply relate to such unique features. In spite of numerous results accumulated on the physiological functions of GSLs and those microdomains [2-6, 9, 10], how GSL microdomains function in membranes and how they modulate membrane properties have been still ambiguous [11], due to variety of species and to small amounts of gangliosides in cells. It would be particularly important to elucidate physicochemical characteristics of ganglioside aggregates since the formation of GSL domains can greatly modify or modulate plasma membrane structures and functions of proteins occluded in membrane, which would relate to the regulation of cell signaling [6, 9].

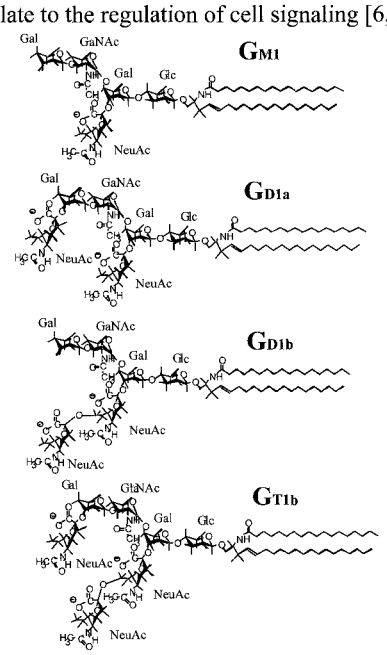

Fig. 1. Schematic representation of molecular structures of G_{M1}, G_{D1a}, G_{D1b}, G_{T1b} gangliosides, respectively

By using synchrotron radiation small-angle X-ray scattering (SR-SAXS), small-angle neutron scattering (SANS) and neutron spin echo (NSE) techniques complementary, we have clarified several notable physicochemical characteristics of the structures and dynamics of ganglioside micelles and ganglioside-containing vesicles, depending on

temperature, pH, salt concentrations, and lipid compositions. We summarize Thus, 1) Gangliosides (monosialoganglioside G_{M1}, G_{M3}; disialogangliosides G_{D1a}, G_{D1b}; trisialoganglioside G_{T1b}) form an ellipsoidal micelle whose sugar-chain regions are very hydrophilic [12]. With elevating temperature, hydration and dehydration of hydrophilic head portion occur with the conformational change of bending of the sugar chain [13-16] and with the change of dissociation degree of sialic acids [17, 18]. These changes accompany some thermal hysteresis that shows the dependence on ganglioside species [19]. 2) In ganglioside (G_{M1})/phospholipid (DPPC, dipalmitoyl phosphocholine) mixed small unilamellar vesicle (SUV) system gangliosides predominantly locate at outer-leaflet of the vesicle as occurring in plasma membrane [20]. 3) In the cases of ganglioside (G_{M1}, G_{D1a}, G_{D1b}, G_{T1b})-cholesterol binary systems (monosialoganglioside, G_{M1}; disialoganglioside, G_{D1a}, IV^3NeuAc-, II^3NeuAc-$GgOse_4$-Cer; disialoganglioside, G_{D1b}, II^3NeuAc_2-$GgOse_4$-Cer; trisialoganglioside, G_{T1b}, IV^3NeuAc-, II^3NeuAc_2-$GgOse_4$-Cer) we found the presence of maximum miscibility of cholesterols within gangliosides, the cholesterol-dependent micelle-to-vesicle transitions (G_{M1}), and the Ca-induced vesicle-to-lamellar transitions (G_{M1}) accompanying the formation of an interdigitated structure between the sugar heads in the opposing bilayers [21]. 4) From the NSE experiments, the dehydration and the bending of sugar heads suppress the undulation of the ganglioside micellar structure [22]. In the case of ganglioside-cholesterol- phospholipid (DSPC, distearoyl phosphocholine; DOPC, dioleoyl phospho- choline; POPC, palmitoyl-oleoyl phosphocholine; PC, L-α-phosphocholine) ternary SUV systems, the bending modulus tends to take a smallest value at the lipid composition of [ganglioside]/[cholesterol]/[glycerophospholipid]≈ 0.1/0.1/1 as similar extent as in intact neuronal cell including rafts, meaning that the ganglioside-cholesterol microdomains can afford an appropriate fluidity to membrane and to hold a homeostasis of membrane environments [23]. It should be noticed that hydrophilic environments afforded by gangliosides are assumed to have a pivotal role in some protein activity. Actually, a hydrophilic environment afforded by gangliosides is assumed to have a pivotal role in some protein activity. It has shown that gangliosides have inhibitory effects on phospholipase A_2 [24] and C [25] activities and that the phospholipase activity is concurrent with a dehydration process of membrane interfaces [26]. These results suggest that the existence of a high capacity of gangliosides to structure water plays a major role in those inhibitory effects [27]. On the other hand, our recent experiments show that the presence of in ganglioside-cholesterol-DPPC ternary mixture enhances the heterogeneity of lipid distribution within the bilayer due to the clustering of ganglioside and cholesterol, namely, the formation of ganglioside-cholesterol rich microdomains [27]. Thus these previous results found on the physicochemical properties of ganglioside aggregates and those mixtures with other lipids suggest that the microdomains enriched in ganglioside and cholesterol can not only modulate locally charge and hydrophilicity of plasma membrane surfaces but also dominates dynamics of plasma membrane, which are essentially important for transmembrane signaling such as the accumulation and activation of functional proteins.

In spite of the use of solution X-ray and neutron scattering methods for the unordered dispersion systems of micelles and vesicles without multilayered structures, we have obtained the above enhanced information on lipid aggregate interfaces. The present report is focused on the methods of SAXS and SANS data analyses for characterizing the interfacial structure of micelle and vesicle systems with referring our previous reports.

2. EXPERIMENTAL

2.1 Sample Preparation

Gangliosides studied (G_{M1}, G_{D1a}, G_{D1b}, G_{T1b}) were from bovine brain purchased from SIGMA Chemical Co. (USA), which were used without further purification. Cholesterol and different types of phospholipids (DPPC, DSPC, DOPC, POPC, PC) purchased from SIGMA Chemical Co. and from Avanti Polar Lipids Inc. (USA) were used without further purification. All other chemicals used were of analytical grade. For the preparation of ganglioside-cholesterol-phosphlipid ternary mixed samples, required quantities of ganglioside, cholesterol and phospholipid were dissolved in a 2:1 (v/v) mixture of chloroform and methanol. The solvent was removed in a stream of nitrogen gas, and the samples were dried at 45 °C in vacuo for overnight. The dried samples were suspended in 50 mM HEPES (*N*-(2-hydroxymethyl) piperazine-*N'*-(2-ethane-sulfonic acid)) H_2O buffer adjusted to pH 7, and the mixture was stirred for several minutes. For the preparation of the small unilamellar vesicle (SUV) samples the dried mixtures were suspended in 50 mM Hepes buffer (pH 7.0), warmed to 45 °C, and stirred at 50 °C for several minutes. The mixtures were sonicated for 10 minutes at 45°C by using a high-power probe-type ultrasonicator (Model UH-50 of SMT Co.) at 50 W. These solutions were incubated for 2 hours at 45 °C, and kept at 4 °C for ~12 hours before scattering measurements. For the employment of the inverse contrast variation method in SANS experiments, we used both hydrated and deuterated DPPC. Namely, 1,2-Dipalmitoyl-*sn*-glycero-3-phosphocholine (h-DPPC) and 1,2-dipalmitoyl-d62-*sn*-glycero-3- phosphocholine (d-DPPC) purchased from Avanti Polar Lipids Inc. (USA). The SUVs were dissolved the in 99.9+ atom % D_2O solvent with 50 mM Hepes adjusted to pH 7. The contrast of the SUV to D_2O solvent was varied by changing the molar ratio of [h-DPPC]/[d-DPPC] which were 1/0, 0.72/0.28, 0.32/0.68 and 0/1. The molar ratio of [G_{M1}]/[cholesterol]/[DPPC] was fixed at 0.105/0.105/1. The total lipid concentration was 1 % w/v for all samples. The molar ratios between h-DPPC and d-DPPC was 1/0, 0.3/0.7, 0.7/0.3 and 0/1. These samples with different [h-DPPC]/[d-DPPC] ratios were served for SANS, SAXS and DLS experiments. Before scattering measurements the sample solutions were filtered with a membrane filter of 0.1 μm pore-size from Whatman Co. (UK).

2.2 X-ray and Neutron Scattering Experiments

Small-angle X-ray scattering (SAXS) experiments were carried out by using a SAXS spectrometer installed

at the synchrotron radiation source (PF) at the High Energy Accelerator Research Organization (KEK), Tsukuba, Japan. The X-ray wavelength, the sample-to-detector distance and the exposure time were 1.49 Å, 190 or 85 cm, and 60-300 seconds, respectively. Other measurement conditions were same as those of the previous experiments [13-19, 23]. Small-angle neutron scattering (SANS) measurements were carried out by using a SANS spectrometer installed at the research reactor JRR-3M of Japan Atomic Energy Agency (JAEA), Tokai, Japan. The neutron wavelength was 7.0 Å. The sample to two-dimensional area detector distance was 2 m and 8 m, which covered q-range from 0.005 $Å^{-1}$ to 0.15 $Å^{-1}$. The exposure time was 60 minutes [20, 23, 28].

3. RESULTS AND DISCUSSION

3.1 Internal Structure, Hydration, Effective Surface Charge of Micelles

For mono-dispersion systems containing identical globular particles such as micelles we are able to determine the internal structure of the solute particle by using a model fitting analysis. Based on the convolution theory, the scattering function of a globular particle with a center symmetric scattering density distribution, such as a micelle, is simply given by that of a multi-shelled ellipsoid of rotation [12, 28]. As shown previously [12-14], the spherical averaged form factor $I_s(q,R)$ of a particle of ellipsoid of rotation (the outer-radius R) composed of n shells with different average scattering densities is given by the following equation.

$$I_s(q,R)=\int_0^1\left[3\left\{\overline{\rho}_1 V_1 j_1(qR_1)/(qR_1)+\sum_{i=2}^{n}(\overline{\rho}_i-\overline{\rho}_{i-1})V_i j_1(qR_i)/(qR_i)\right\}\right]^2 dx \quad (1)$$

where N is the number concentration of the particles, is the average excess scattering density (so-called contrast) of i th shell with a shape of an ellipsoid of rotation, j_1 the spherical Bessel function of the first rank. R_i is defined as

$$R_i=r_i\left\{1+x^2(\nu_i^2-1)\right\}^{1/2} \quad (2)$$

where r_i and n_i are the semiaxis and its ratio of i th ellipsoidal shell, respectively. Equation 4 is well applicable to fit the experimental scattering data of ganglioside micellar solutions with the theoretical scattering functions as shown in Figure 1, where Figure 1A shows the experimental SAXS curves of GM1 and GD1a micelles at 25 °C, pH7, the best fitted theoretical scattering curves from hard sphere model, hard ellipsoid model, and double-shelled ellipsoid model, respectively.

As reported previously [16, 19] we can evaluate the number n_W of water molecules occluded in the hydrophilic shell region by using the following equation based on the values of structural parameters obtained from the shell-modeling analysis.

$$n_W=\left[\left\{\frac{\Delta_{shell}}{\Delta_{core}}\left(\frac{\Sigma_{tail}b}{V_{tail}}-\alpha\right)+\alpha\right\}V_{shell}-n_a\Sigma_{head}b\right]/\Sigma_{water}b \quad (3)$$

where $\Sigma_{water}b$, $\Sigma_{head}b$, $\Sigma_{tail}b$, V_{water}, V_{head}, V_{tail} are the total scattering amplitudes and the excluded volumes of water molecule, the head and tail portions of the lipid molecule, respectively; $\alpha=\Sigma_{water}b/V_{water}=9.4\times10^{10}\,cm^{-2}$. As we know the chemical components water molecule, hydrophilic head and hydrophobic tail portions of lipid molecule, we can calculate, for examples, $\Sigma_{water}b=2.81\times10^{10}\,cm^{-2}$, $\Sigma_{head}b=1.50\times10^{10}\,cm^{-2}$ for G_{M1}, $\Sigma_{head}b=1.92\times10^{10}\,cm^{-2}$ for G_{D_1}, and $\Sigma_{tail}b=8.69\times10^{10}\,cm^{-2}$ for the ceramide portion of ganglioside. n_a is the aggregation number of ganglioside micelles estimated by $n_a=V_{core}/V_{tail}$; $\Delta_{shell}/\Delta_{core}$ is the ratio between the shell and core contrasts, which are obtained from the structural parameters of the shell-modeling analysis. We found that the sugar head portion can occlude amounts of water (~120 water molecules/G_{M1}, ~200 water molecules/G_{D1} at 6 °C) that decreases with elevation of temperature (~50 water molecules/G_{M1}, ~100 water molecules/G_{D1} at 65 °C).

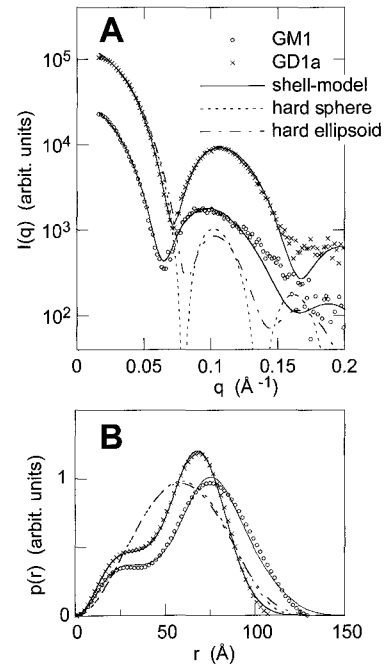

Fig. 2. A, the experimental and theoretical SAXS curves of G_{M1}, G_{D1a} ganglioside micelles at 25 °C, pH 7 (0.5 % w/v); B, those distance distribution functions. The marks show experimental data.

Especially for a charged particle system at high concentration an effect of repulsive interparticle interaction appears occasionally in the small-angle region of observed scattering data. In such cases we use the scattering function of identical particles interacting with each other is generally given by

$$I(q,R)\propto NI_s(q,R)S(q) \quad (4)$$

where $S(q)$ the interparticle structure factor obtained by Fourier transforming the interparticle correlation function. According to the scheme of the rescaled mean spherical approximation the $S(q)$ for identical macroions interacting through a repulsive screened Coulomb potential is given as

$$S(q)=1/\{1-24\eta a(q\sigma)\} \quad (5)$$

where $\eta = \pi N\sigma^3/6$ is the volume fraction occupied by the particles, σ the effective particle diameter, $a(q\sigma)$ the function defined by Hayter and Penfold [29]. By using Equation 6 we can determine both the effective charge and internal structure of the micelles, as shown in Figure 3 [17, 18]. Thus, in our previous papers [17, 18], we treated a repulsive interaction between disialoganglioside G_{D1} micellar systems and found that the elevation of temperature induces both the effective surface charge and internal structure of the micelles.

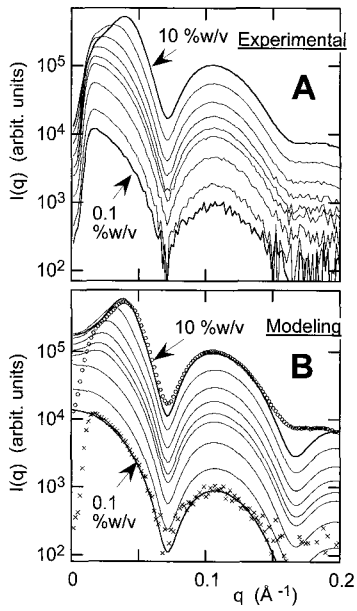

Fig. 3. A, SAXS curve of G_{D1a} ganglioside micelle depending on concentration from 0.1 % w/v to 10 % w/v at 25 °C, pH 7; B, simulated theoretical SAXS curve with the experimental ones at 0.1 and 10 % w/v indicated by the marks. The full lines in B show the theoretical ones.

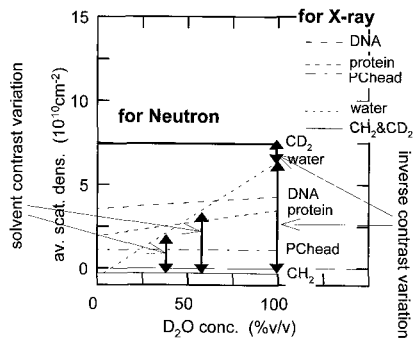

Fig. 4. Average scattering densities of some representative biological components for neutron and X-ray. The contrast variation methods (solvent contrast variation and inverse contrast variation for neutron) are shown schematically.

3.2 Asymmetric Bilayer Structure of Uni-lamellar Vesicle: Use of SANS Inverse Contrast Variation -I-

When the effect of the repulsive interaction on the small-angle scattering data, such as shown Figure 3, can be neglected experimentally, the shell-modeling method combined with a size distribution function is applicable to determine both the internal structure and size distribution of the uni-lamellar vesicle by fitting the experimental SANS and SAXS scattering curves with the theoretical ones. Vesicle solutions are ordinary polydisperse, therefore, the scattering function $I(q)$ is given by

$$I(q) \propto \int_{R_{min}}^{\infty} I_s(q,R) D(R) dR \tag{6}$$

where $D(R)$ is the size distribution function of the particle radius R, and $I_s(q,R)$ is the form factor of the particle given by Equation 1. R_{min} is a lower limit of particle radius determined by the bilayer thickness of the SUV. For a particle composed of spherical shells, the form factor given by Equation 1 is simplified as [20]

$$I_s(q,R) = 9\left\{\bar{\rho}_1 V_1 j_1(qR_1)/(qR_1) + \sum_{i=2}^{n} (\bar{\rho}_i - \bar{\rho}_{i-1}) V_i j_1(qR_i)/(qR_i)\right\}^2 \tag{7}$$

As a number distribution function of particle radii $D(R)$, we adopted the following Gaussian distribution function which is used in many cases of SUV systems [30].

$$D(R) = \frac{1}{\sqrt{2\pi}\sigma} \exp\left\{-\frac{(R-\bar{R})^2}{2\sigma^2}\right\} \tag{8}$$

where $\bar{R}$ and σ are the average radius and the standard deviation, respectively. By using Equation 8 we describe fit well the experimental scattering function with the theoretical one, and can determine both the size-distribution function and the bilayer structure of the SUV. On the other hand, the concept of 'contrast' (average excess scattering density of solute particle from that of solvent) is essentially important for solution scattering methods. Figure 4 shows the average scattering densities of representative biological components for neutron and X-ray. For a precise modeling analysis it is important to obtain scattering data from a same particle at various contrasts. In the case of SANS the contrast variation method is used to observe a scattering object at different contrasts, namely, at different phases. To avoid background incoherent scattering from protons and an artifact caused by H-D exchange in the solvent contrast variation method, the inverse contrast variation method is very useful, where the contrast is varied by the deuteration ratio of solute particles, not by H_2O/D_2O ratio in water solvent, as shown in Figure 4. The inverse contrast variation method is a powerful method to clarify an asymmetric structure or a heterogeneous structure of bilayer within lipid membrane composed of different molecules. For example, the asymmetric distribution of ganglioside molecules within [ganlioside G_{M1}]/[DPPC]=0.1/1 mixed SUV vesicle bilayer has been clarified [20]. Figure 5 shows the SANS curve depending on the inverse contrast, where the contrast was varied by changing the molar ratio between [d-DPPC (deuterated DPPC)]/[h-DPPC (protonated-DPPC)] from 1/0, 0.7/0.3, 0.3/0.7 to 0/1. In addition SAXS curves of these four vesicle samples were measured. In spite of the variation of SANS curve depending on the inverse contrast variation, all SAXS curves agree with each other, suggesting that all SUV samples with different [d-DPPC]/[h-DPPC] ratios are same for X-ray. Alternatively, it means that we successfully observed the scattering curve from the vesicle at five different contrasts (phases), namely, at four of them from neutron

and at one of them from X-ray. Based on Equation 8, all SANS and SAXS curves can be described by the theoretical scattering functions of a unique SUV model at different contrasts, as shown by the full lines in Figure 5.

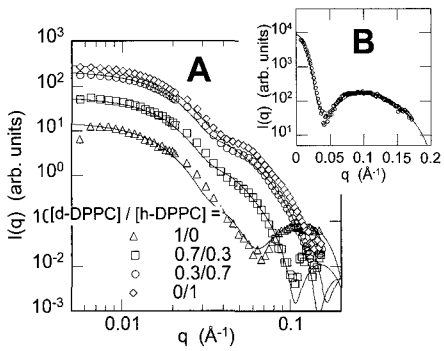

Fig. 5. A, SANS curve of [ganglioside]/[DPPC]= 0.1/1 SUV depending on inverse contrast variation; B, SAXS curve of the same SUV. The marks and full lines correspond to the experimental data and the best-fitted theoretical scattering functions of the model shown in Figure 6.

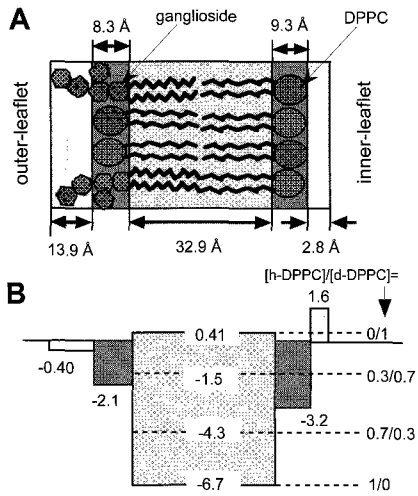

Fig. 6. Asymmetric bilayer structure of [ganglioside] /[DPPC]=0.1/1 SUV determined by the inverse contrast variation at 25 °C. A, thickness of each region; B, contrast profile within the bilayer.

The obtained model, shown in Figure 6, clearly shows that ganglioside molecules preferentially localize at the outer-leaflet of the SUV bilayer. The sugar chain region at the outer-leaflet of the bilayer was dehydrated with the conformational change by elevating temperature, as similarly observed in the ganglioside micellar systems.

3.3 Microdomain Formation within Bilayer of Uni-lamellar Vesicle: Use of SANS Inverse Contrast Variation -II-

Some heterogeneous distribution of lipid compositions within a SUV bilayer, such as lipid microdomains composed of ganglioside and cholesterol, can be clarified by using the inverse contrast variation [31]. In the case of ganglioside-cholesterol-DPPC ternary lipid mixture, the zero-angle scattering intensity $I(0)$, determined by the extrapolation of the Guinier plot ($\ln I(q)$ versus q^2 plot) to zero-angle, is given as

$$[I(0)]^{1/2} \propto \left\{\hat{\rho}_H V_{head} + (\bar{\rho}_T^H - \bar{\rho}_S)V_{tail} - \bar{\rho}_S V_{core}\right\} + a(\bar{\rho}_T^D - \bar{\rho}_T^H)V_{tail} \quad (9)$$

where a is the deuteration ratio defined by [d-DPPC]/[total DPPC]; $\hat{\rho}_H$, $\bar{\rho}_T^H$, $\bar{\rho}_T^D$, ρ_S are the contrast of the head region, the average scattering densities of the tail regions of h-DPPC and d-DPPC, the average scattering density of the solvent; V_{head}, V_{tail} and V_{core} are the volumes of the head, tail and core (water pool) regions of the SUV, respectively. From the linear relation between $[I(0)]^{1/2}$ and a we can determine experimentally the contrast matching point of the SUV by extrapolating the slope to the abscissa to satisfy $[I(0)]^{1/2}=0$. The value of the matching point is given by the unit of the d-DPPC molar ratio for the case of the inverse contrast variation, not by the D_2O content of solvent for the case of the solvent contrast variation. From the matching point the value of the contrast can be defined in the unit of the d-DPPC molar ratio. The radius of gyration R_g is derived as

$$R_g^2 = R_{g0}^2 + \frac{\alpha}{\hat{\rho}V} - \frac{\beta}{(\hat{\rho}V)^2} \quad (10)$$

where the factors α and β are

$$\alpha = \int_V \rho_{vesicle}^F(\mathbf{r})\mathbf{r}^2 d\mathbf{r}, \quad \beta = \left\{\int_V \rho_{vesicle}^F(\mathbf{r})\mathbf{r}d\mathbf{r}\right\}^2 \quad (11)$$

In the equations 10 and 11 $\rho_{vesicle}^F(\mathbf{r})$, V and R_{g0} are the scattering density fluctuation within the vesicle from its average contrast $\hat{\rho}$, the vesicle volume and the R_g at a infinite contrast, respectively. Figure 7A shows the dependence of $[I(0)]^{1/2}$ on the molar ratio a of d-DPPC against total DPPC for determining the contrast matching point. In Figure 7B the R_g^2 is plotted against the inverse of $\hat{\rho}$, which we call a pseudo Stuhrmann-plot. According to the analogy of so-called Stuhrmann-plot, the large negative slope in Figure 7B results from the negative value of α of the second term in Equation 12, reflecting an asymmetric scattering density distribution with a negative contrast at outside of a solute particle. Alternatively, in the present case ganglioside and cholesterol molecules are preferentially distributed at the outer leaflet of SUV. The deviation from the linearity in Figure 7B is attributable to the third term of Equation 12, that is, the center of gravity of the scattering density distribution of SUV is shifted from the geometrical center of SUV. This clearly indicates that in the case of SUV the ganglioside-cholesterol rich domains are distributed heterogeneously on the outer-leaflet of bilayer membrane. The elevation of temperature enhances such a deviation, meaning the growth of the microdomains.

On the contrary, in the case of the SUV of cholesterol-DPPC binary mixture the deviation from the linearity in the pseudo Stuhrmann-plot is smaller than that of the above ternary mixture, and the elevation of temperature reduces a deviation. These facts clearly show an essential role of gangliosides on the formation of lipid microdomains within the bilayer membrane. Other recent study of the effect of monovalent cations (Na^+ and K^+) on the permeability of water across the membrane of ganglioside (G_{D3}) /cholesterol/phospholipid mixtures by using time-resolved SANS and SAXS methods the permeability is greatly enhanced by K^+ ion, suggesting

the function of the G_{D3}/cholesterol rich clusters on neuronal excitations by K^+ [32].

As we have shown in the above results so far, the complementary use of SAXS and SANS methods is able to afford us fruitful information on various functional properties of raft model membrane by applying advanced analyses to experimental data. The specificity of the interaction between GSL aggregates and proteins depending on sugar chains was also clarified using SANS and SAXS [33]. A direct observation of membrane interfaces using X-ray or neutron reflection measurements would be further promising to clarify various events occurring in biomembrane surfaces, which is now planning.

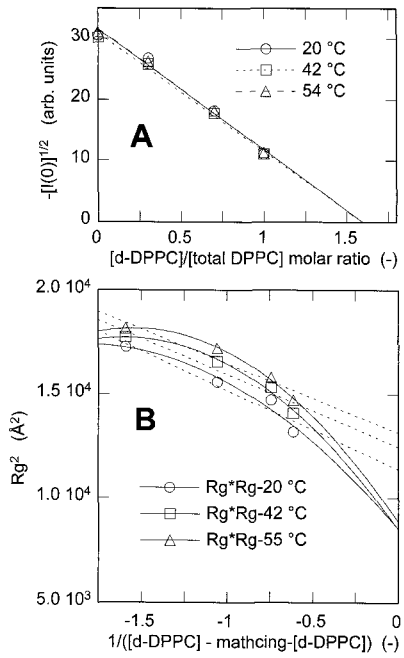

Fig. 7. Microdomain formation of [ganglioside] /[cholesterol]/[DPPC]=0.1/0.1/1 SUV analysed by using the inverse contrast variation. A, square of zero-angle scattering intensity depending on the deuteration ratio; B, pseudo Stuhrmann-plot.

References

[1] K. Simons and E. Ikonen, *Nature,* **387**, 569-572 (1997).

[2] S. Hakomori, K. Handa, K. Iwabuchi S.Yamamura and A. Prinetti, Glycobiology, 8, xi-xix (1998).

[3] K. Simons and D. Toomre, *Nat. Rev. Mol. Cell Biol.* **1**, 31 -39 (2000).

[4] L. Svennerholm et al., "*Biological Function of Gangliosides*", Elsevier, Amsterdam (1994).

[5] R. W. Ledeen, S. Hakomori, A. J. Yates, J. S. Schneider and R. K. Yu, "*Sphingolipids as signaling modulators in the nervous system*", The New York Academy of Sciences, New York (1998).

[6] S. Hakomori, *Trends Glycosci. Glycotechnol.*, **13**, 219-230 (2001).

[7] I. Pascher, *Biochim. Biophys. Acta*, **455**, 433-451 (1976).

[8] A. Ferraretto, M. Pitto, P. Palestin, and M. Masserini, *Biochemistry,* **36**, 9232-9236 (1997).

[9] K. Kasahara, K. Watanabe, K. Takeuchi, H. Kaneko, H., A. Oohira, T. Yamamoto and Y. Sanai, *J. Biol. Chem.,* **275,** 34701–34709 (2000).

[10] K. Yuyama, N. S-Suzuki, Y. Sanai and K. Kasahara, *Trends Glycosci. Glycotechnol.*, **15**, 139-151 (2003).

[11] H. Heerklotz, *Biophys. J.*, **83**, 2693-2701 (2002).

[12] M. Hirai, S. Yabuki, T. Takizawa, Y. Nakata, H. Mitomo, T. Hirai, S. Shimizu, K. Kobayashi, M. Furusaka, and K. Hayashi, *Physica B*, **213&214**, 748-750 (1995).

[13] M. Hirai, T. Takizawa, S. Yabuki, Y. Nakata and K. Hayashi, *Biophys. J.*, **7**, 1761-1768 (1996).

[14] M. Hirai, T. Takizawa, S. Yabuki, T. Hirai and K. Hayashi, *J. Phys. Chem.*, **100**, 11675-11680 (1996).

[15] M. Hirai, S. Arai, T. Takizawa, S. Yabuki and Y. Nakata, *Thermochim. Acta.*, **308**, 93-99 (1998).

[16] M. Hirai and T. Takizawa, *Biophys. J.*, **74**, 3010-3014 (1998).

[17] M. Hirai and T. Takizawa, S. Yabuki and K. Hayashi, *J. Chem. Soc. Faraday Trans.* **92**, 4533-4540 (1996).

[18] M. Hirai, H. Iwase, H. and T. Hayakawa, *J. Phys. Chem. B.* **103**, 10136-10142 (1999).

[19] T. Hayakawa and M. Hirai, *Eur. Biophys. J.* **31**, 62-72 (2002).

[20] M. Hirai, H. Iwase, T. Hayakawa, M. Koizumi and H. Takahashi, H. *Biophys. J.* **85**, 1600-1610 (2003).

[21] T. Hayakawa and M. Hirai, *J. Appl. Cryst.* **36**, 489-493 (2003).

[22] M. Hirai, H. Iwase and T. Hayakawa, *J. Phys. Soc. Jpn*, **70**, 420-423 (2001).

[23] M. Hirai, M. Koizumi, H. Hirai, T. Hayakawa, K. Yuyama, N. Suzuki and K. Kasahara, *J. Phys.: Condens. Matter*, **17**, s2965-s2977 (2005).

[24] Maggio, B., I. D. Bianco, G. G. Montich, G. D. Fidelio, and R. K. Yu, *Biochim. Biophys. Acta.*, **1190**, 137-148 (1994).

[25] J. J. Daniele, B. Maggio, I. D. Bianco, F. M. Goni, A. Alonso, and G. D. Fidelio, *Eur. J. Biochem.*, **239**, 105-110 (1996).

[26] M. K. Jain, J. Rogers, G. H. DeHaas, *Biochim. Biophys. Acta.*, **940**, 51-62 (1988).

[27] C. Arnulphi, P. R. Levstein, M. E. Ramia, C. A. Martin, and G. D. Fidelio, *J. Lipid Res.*, **38**, 1412-1420 (1997).

[28] M. Hirai, T. Hirai and T. Ueki, *Macromolecules*, **27**, 1003-1006 (1994).

[29] J. B. Hayter, J. Penfold, *Molec. Phys.*, **42**, 109-118 (1981).

[30] P. Balgavy, M. Dubnickova, N. Kucerka, M. A. Kiselev, S. P. Yaradaikin, and D. Uhrikova, *Biochim. Biophys. Acta,* **1512**, 40-52 (2001).

[31] M. Hirai, H. Hirai, M. Koizumi, K. Kasahara, K. Yuyama, and N. Suzuki, *Physica B*, 385&386, 868-870 (2006).

[32] M. Hirai, T. Onai, M. Koizumi, H. Hirai, K. Kasahara, K. Yuyama, N. Suzuki, and K. Inoue, *J. Appl. Cryst.* **40**, in press (2007).

[33] M. Hirai, H. Iwase, S. Arai, T. Takizawa and K. Hayashi, *Biophys. J.*, **74**, 1380-1387 (1998).

(Received December 9, 2006;Accepted January 29, 2007)